EPJ manuscript No.
(will be inserted by the editor)

The Structure of the Nucleon: Elastic Electromagnetic Form Factors

V. Punjabi[1], C.F. Perdrisat[2], M.K. Jones[3], E.J. Brash[3,4], and C.E. Carlson[2]

[1] Norfolk State University, Norfolk, VA 23504, USA
[2] The College of William & Mary, Williamsburg, VA 23187, USA
[3] Thomas Jefferson National Accelerator Facility, Newport News, VA 23606, USA
[4] Christopher Newport University, Newport News, VA 23606, USA

Received: November 26, 2014/ Revised version: November 26, 2014

Abstract. Precise proton and neutron form factor measurements at Jefferson Lab, using spin observables, have recently made a tremendous contribution to unraveling of the internal structure of the nucleon. Accurate experimental measurements of the nucleon form factors are a testbed for understanding how their static properties and dynamical behavior emerge from QCD, the theory of the strong interactions between quarks. There has been enormous theoretical progresses since the publication of the Jefferson Lab proton form factor ratio data, aiming at reevaluating the picture of the nucleon. We will review the experimental and theoretical progress, such as generalized parton distributions and flavor separation, Dyson-Schwinger equations (DSEs) calculations, improvements made in lattice QCD calculations, and more.

PACS. PACS-key describing text of that key – PACS-key describing text of that key

1 Introduction

Nucleons are the building blocks of almost all ordinary matter in the universe. The challenge of understanding the nucleon's structure and dynamics has occupied a central place in nuclear physics. The nucleon (proton and neutron) electromagnetic form factors describe the spatial distributions of electric charge and current inside the nucleon, hence are intimately related to its internal structure; these form factors are among the most basic observables of the nucleon.

Quantum chromo dynamics (QCD) is the theory of the strong interaction, which is responsible for binding quarks through the exchange of gluons to form hadrons (baryons and mesons). The fundamental understanding of the nucleon form factors in terms of QCD is one of the outstanding problems in nuclear physics. Why do quarks form colorless hadrons with only two stable configurations, proton and neutron? One important step towards answering this question is to characterize the internal structure of the nucleon. High energy electron scattering provides one of the most powerful tools to investigate this structure.

Early electron scattering experiments with nuclei were motivated by a need to verify predictions of the then current models of the electromagnetic interaction of electrons with nuclei, and in particular with the proton and neutron; Rosenbluth predicted that high energy electrons would be scattered dominantly by the magnetic moment of the proton [58]. Available accelerators in the early fifties had energies smaller than 50 MeV, and provided much information on the nuclear radius of elements from Be to Pb. First clear evidence that the proton was not point like was obtained at the Stanford accelerator in the period 1953-1956, under the leadership of Robert Hofstadter. Clear demonstration that the proton has a finite size (unlike the electron?) had to wait for the availability of electron beams with higher energy, like the 550 MeV Stanford linear accelerator. In his extensive, 1956 review Hofstadter [43] discussed data for the angular distribution of the elastically scattered electrons up to 140 degrees; these data differ from the expectation for a point charge and magnetic distribution by a factor of five at the largest $q^2 = 14 \times 10^{-26}\ cm^{-2} = 14\ fm^{-2}$ or $\approx 0.73\ GeV^2$. A proton radius of 0.77±0.1 fm was derived from the momentum transfer squared q^2 dependence of a form factor $F^2(q^2)$ defined in terms of the charge density distribution as:

$$\rho(r) = \frac{1}{2\pi^2 r} \int F(q) sin(qr) q dq. \quad (1)$$

In 1957 Yennie, Levy and Ravenhall [28] derived an expression for the **ep** cross section in terms of two form factors, F_1 and F_2, following Rosenbluth's work, as:

$$\sigma(\theta) = \sigma_{NS} \left\{ F_1^2 + \frac{q^2}{4M^2} \left[2(F_1 + F_2)^2 \tan^2 \frac{\theta_e}{2} \right] \right\}, \quad (2)$$

where F_1 was introduced to represent the spread-out charge and spread-out Dirac magnetic moment. F_2 describes the

Send offprint requests to:

spread-out Pauli (or anomalous) magnetic moment. σ_{NS} is equal to the Mott cross section corrected for the nucleon recoil (see Eq. 8 below).

A similar change in accepted concepts occurred when the JLab data for the proton form factor ratio $\mu_p \frac{G_{Ep}}{G_{Mp}}$ from double polarization experiments, completed in 2000 up to Q^2 of 5.8 GeV^2, differed drastically from the form factor results obtained using the Rosenbluth separation method; here μ_p is the magnetic moment of the proton. The standard data base up to this time had been entirely defined by cross section measurements, and suggested that, for $Q^2 <\sim 10GeV^2$, both the electric and magnetic form factors behaved approximately like the dipole form factor:

$$G_D = \left(1 + \frac{Q^2}{0.71}\right)^{-2}, \tag{3}$$

with the four momentum transfer squared $Q^2 = -q^2 = -(\boldsymbol{q}^2 - \omega^2)$; $\boldsymbol{q}$ the vector polarization transfer and ω the energy transfer, in units of GeV^2.

What the series of experiments started in 1998 in Hall A at JLab demonstrated was that the electric and magnetic form factor ratio $\mu_p \frac{G_{Ep}}{G_{Mp}}$ decreased approximately linearly with Q^2, reaching a value of 1/3.7 times the value at $Q^2 = 0$ at the highest Q^2 investigated at that time, 5.6 GeV^2. Coincidentally, Rosenbluth [58] had argued in 1950, that in a combination of the spread-out electric charge produced by the pion cloud and the strongly anomalous magnetic moment of the proton, the magnetic form factor would dominate the data at large Q^2; fifty years later this "prediction" was verified by the JLab data. And almost 60 year after the work of ref. [43] the question of whether the proton radius is ≈ 0.877 or 0.8409 fm, a difference of 6.9 standard deviations, is being discussed intensely.

1.1 History of elastic electron scattering on the nucleon

Elastic electron proton scattering has evolved since the history making series of experiments with electron beams at the Stanford Linear Accelerator in 1956. Under the leadership of R. Hofstadter, a series of crucial results were obtained from cross section measurements [44]. Several fundamental pieces of information were established following these experiments, including the approximate $1/Q^8$ decrease of the cross section with the invariant four momentum transfer squared, Q^2, establishing the approximate shape of the charge distribution, and a first value for the proton radius. Theoretical work evolved in parallel with these experimental "firsts", leading to the description of the elastic electron scattering process in terms of the lowest order process, the exchange of a single virtual photon with negative invariant mass squared; this lowest order contribution, also called the Born term, was expected to be dominant because of the smallness of the electromagnetic coupling constant α_{EM}. Fundamental expressions for the hadronic current and the definition of two invariant form factors, F_1 and F_2, later named the Dirac and Pauli form factors, of the Born (single photon exchange) term, were issues of this period. Experimenters use preferably the Sachs form factors G_E and G_M, which are linearly related to F_1 and F_2

$$\begin{aligned} G_{E_{p,n}} &= F_{1_{p,n}} - \tau F_{2_{p,n}} \\ G_{M_{p,n}} &= F_{1_{p,n}} + F_{2_{p,n}}, \end{aligned} \tag{4}$$

.

The possibility of observing polarization transfer, or asymmetry, for longitudinally polarized electrons, measuring either the polarization transferred to the recoil proton, or the asymmetry if the target proton or neutron is polarized, was first discussed in a paper by Akhiezer et al [4]. It was to be more than 20 years before such experiments, which require a polarized electron beam, could be performed with good accuracy. Further papers on double polarization experiments followed, including Akhiezer and Rekalo [3], and Dombey [61]. The accidental time coincidence of the initial phase of the construction of the CEBAF accelerator at the Thomas Jefferson National Accelerator Facility (TJNAF) or JLab, in Virginia, and a paper by Arnold, Carlson and Gross [68] about double polarization experiments, lead to an intensive program of nucleon form factor experiments and a significant breakthrough in our understanding of the proton structure. A series of double-spin experiments, first for the proton and then for the neutron, followed, with conundrum changing consequences.

In the Born approximation the transferred polarization has only two components, both in the reaction plane defined by the beam and scattered electron, one along the recoil proton momentum, and the other perpendicular to it. For the proton, polarization transfer has been used most often at JLab for the proton; it requires a rescattering of the proton to measure its polarization, and is dependent on the analyzing power of the reaction used. For the neutron, target asymmetry has now been used successfully [71] for the determination of the G_{En}/G_{Mn} ratio; this requires a polarized target of either D_2 or He^3, which limits the maximum electron current that can be tolerated without significant depolarization of the target. Recent progress in the design and construction of polarized liquid ^{3}He-target [32] indicates that future experiments on the neutron form factors should benefit of much increased beam luminosity (at Mainz and JLab). Solid polarized proton targets also reach high polarization by Dynamic Nuclear Polarization, but suffer from beam current limitations, which mitigate some of their advantage over liquid ^{3}He target because of the absence of nuclear effects.

Among the earliest *ep* published polarization experiments, a search in 1963 at the Saclay Linear Accelerator with a beam of 950 MeV electrons, for a symmetry breaking induced recoil polarization perpendicular to the scattering plane, for unpolarized beam electrons and unpolarized target protons, may well have been the first polarization experiment ever performed. Such an effect would be due to the interference of the Born amplitude with the two-photon exchange amplitude in elastic *ep* scattering.

The asymmetry obtained in the vertical plane at Q^2=0.61 GeV^2 was 0.040 ± 0.027 [16].

A similar single-spin experiment in 1970 with an unpolarized 15-18 GeV electron beam at the Stanford linear accelerator, and a polarized proton target with polarization perpendicular to the reaction plane to characterize the interference of the two-photon exchange with the single photon exchange (Born) process, produced asymmetries of order 0.5% in the range of Q^2 0.38 to 0.98 GeV^2.

The early nineties saw a number of double polarization experiments at NIKHEF [46] and MAMI [22,59] to determine the neutron electric form factor up to Q^2 ∼1 GeV^2. All used polarized electron beams and a polarized target, either deuterium or ^3He.

The next step was the measurement of the transverse, in plane recoil proton polarization P_t (or P_x) for longitudinally polarized electrons and unpolarized target in the mid nineties, at the Mainz Microtron (MAMI) [34,77]. This experiment measured the proton form factor ratio G_{Ep}/G_{Mp} up to Q^2 of 0.5 GeV^2, and the results were in agreement with the dipole form factor, $G_D = (1+\frac{Q^2}{0.71})^{-2}$.

The start in 1998 of the recoil polarization program at JLab, both for the proton and the neutron, was preceded by experiments at the BATES Linear Accelerator. For the neutron, the pioneering experiment of Madey et al. performed the first recoil polarization measurement of G_{En} at BATES at a Q^2 of 0.255 GeV^2 in 1994 [33]. For the proton the two polarization transfer components P_ℓ and P_t, and the corresponding G_{Ep}/G_{Mp} ratio were measured at Q^2 of 0.38 to 0.50 GeV^2[27,10].

In 2000 the SAMPLE collaboration obtained the vector analyzing power for 200 MeV transversally polarized electrons for the unpolarized proton, which is parity conserving and time-reversal odd, and tests the contribution of two-photon exchange. When compared with the results of Ref. [16], such transverse effects are suppressed by the relativist boost parameter γ. A value of $A = -15.4 \pm 5.4\ ppm$ at Q^2=0.1 GeV^2 was observed in this experiment [13]. +

1.2 Dirac and Pauli form factors

The lowest order approximation for electron nucleon scattering is the single virtual photon exchange process, or Born term. The Born approximation is expected to provide a good lowest order description of elastic eN scattering (with $N = p, n$) because of the weak electro-magnetic coupling of the photon with the charge and the magnetic moment of the nucleon. The amplitude for the process is the product of the four-component leptonic and hadronic currents, ℓ_ν and $\mathcal{J}_\mu$, and can be written as:

$$i\mathcal{M} = \frac{-i}{q_\mu^2}\ell_\mu \mathcal{J}^\mu = \frac{-ig_{\mu\nu}}{q_\mu^2}\left[ie\bar{u}(k')\gamma^\nu u(k)\right]\left[-ie\bar{v}(p')\Gamma^\mu(p',p)v(p)\right] \quad (5)$$

where k, k', p, p' are the the four-momenta of the incident and scattered, electron and proton, respectively, Γ^μ contains all information of the nucleon structure, and $g_{\mu\nu}$ is the metric tensor. To insure relativistic invariance of the amplitude $\mathcal{M}$, Γ^μ can only contain p, p' and γ^μ, besides numbers, masses and Q^2.

The most general form for the hadronic current for the spin $\frac{1}{2}$-nucleon, satisfying relativistic invariance and current conservation, and including an internal structure is:

$$\mathcal{J}^\mu_{hadronic} = ie\overline{\nu}(p')\left[\gamma^\mu F_1(Q^2) + \frac{i\sigma^{\mu\nu}q_\nu}{2M}\kappa_j F_2(Q^2)\right]\nu(p) \quad (6)$$

where M is the nucleon mass, $kappa_j$, with $j = p, n$ the anomalous magnetic moment, in units of the nuclear magneton, $\mu_N = \frac{e\hbar}{2M}$. $Q^2 = \boldsymbol{q}^{\,2} - \omega^2 = -q_\mu^2$, is the negative of the square of the invariant mass q_μ^2 of the virtual photon of negative mass squared, exchanged in the one-photon approximation of eN scattering. The Dirac and Pauli form factors, $F_1(Q^2)$ and $F_2(Q^2)$ are the only structure functions allowed in the Born term by relativistic invariance. As is now the most frequently used notation, $\kappa_j F_2$ $j = p, n$ will be written as F_{2p} and F_{2n}, respectively. In the static limit, $Q^2 = 0$, $F_{1p} = 1$, $F_{2p} = \kappa_p = 1.7928$ and $F_{1n} = 0$ and $F_{2n} = \kappa_n = -1.9130$, for the proton and neutron, respectively.

The Lab frame differential cross section for detection of the electron in elastic ep or en scattering is then:

$$\frac{d\sigma}{d\Omega_e} = \left(\frac{d\sigma}{d\Omega}\right)_{Mott}\frac{E_e}{E_{beam}}\Big(F_1^2(Q^2) + \tau\Big[F_2^2(Q^2) + 2[F_1(Q^2)+F_2(Q^2)]^2\tan^2\frac{\theta_e}{2}\Big]\Big) \quad (7)$$

with $\tau = Q^2/4M_p^2$; $(\frac{d\sigma}{d\Omega})_{Mott}$ is the Mott cross section given by:

$$\left(\frac{d\sigma}{d\Omega}\right)_{Mott} = \frac{\alpha^2\cos^2\frac{\theta}{2}}{4E_{beam}^2\sin^4\frac{\theta}{2}}. \quad (8)$$

The incident electron (beam) and scattered electron energies are labeled E_{beam} and E_e, respectively. The fraction $\frac{E_e}{E_{beam}}$ in Eq. 1.2 is the recoil correction to the Mott cross section Eq. 8.

Experimental cross section data are most easily analyzed in terms of another set of form factors, the Sachs form factors G_E and G_M. The relation between G_E and G_M and F_1 and F_2 for proton and neutron are given in Eq. 4. The scattering cross section Eq. 1.2 can then be written in a much simpler form, without interference term, leading to a separation method for G_E^2 and G_M^2 known as Rosenbluth (or Longitudinal-Transverse) method, as will be seen below. Now the cross section is:

$$\frac{d\sigma}{d\Omega_e} = \left(\frac{d\sigma}{d\Omega}\right)_{Mott}\frac{E_e}{E_{beam}}\frac{1}{1+\tau)}\left(G_{Ep}^2 + \frac{\tau}{\epsilon}G_{Mp}^2\right) \quad (9)$$

where ϵ is the polarization of the virtual photon defined as:

$$\epsilon = \frac{1}{1+2(1+\tau)\tan^2\frac{\theta_e}{2}}, \quad (10)$$

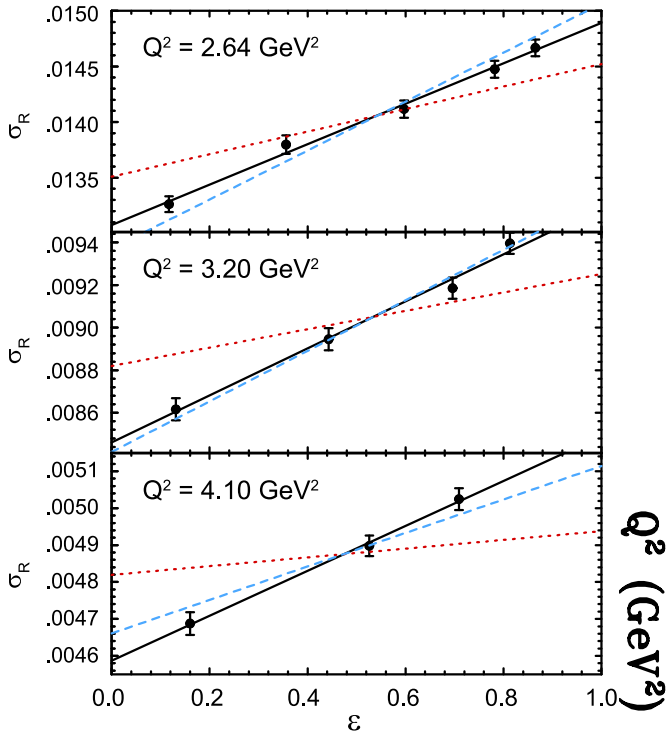

Fig. 1. Illustration of the Rosenbluth separation method to obtain separate values of G_{Ep}^2 and G_{Mp}^2 from the kinematic factor ϵ-dependence of the reduced cross section. Data from Qattan [45]

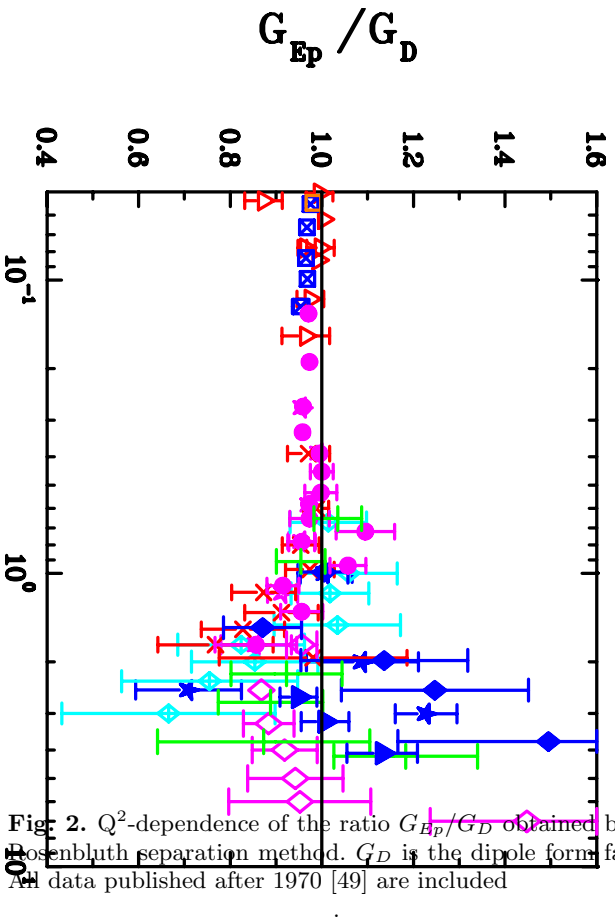

Fig. 2. Q^2-dependence of the ratio G_{Ep}/G_D obtained by the Rosenbluth separation method. G_D is the dipole form factor. All data published after 1970 [49] are included

.

The modern version of the Rosenbluth separation technique takes advantage of the linear dependence in ϵ, in the reduced cross section σ_{red}, based on Eq. (9), as follows:

$$\left(\frac{d\sigma}{d\Omega}\right)_{red} = \epsilon(1+\tau)\frac{E_{beam}}{E_e}\left(\frac{d\sigma}{d\Omega}\right)_{exp} / \left(\frac{d\sigma}{d\Omega}\right)_{Mott} = \tau G_M^2 + \epsilon G_E^2, \quad (11)$$

showing that the reduced cross section σ_{red} is expected to have a linear dependence on ϵ, with slope proportional to G_E^2 and intercept equal to τG_M^2. To illustrate the method, the reduced cross section data, σ_{red}, of ref. [45] are shown in Fig. 1. The corresponding form factor ratios are shown in Fig. 3 on a background of other form factor ratios obtained from Rosenbluth separations. Also shown on this figure are the results of the first two recoil polarization experiments obtained in hall A, triangle symbols. [57,78,62]. The dichotomy between cross section (Rosenbluth separation) and recoil polarization results is very obvious indeed from this figure.

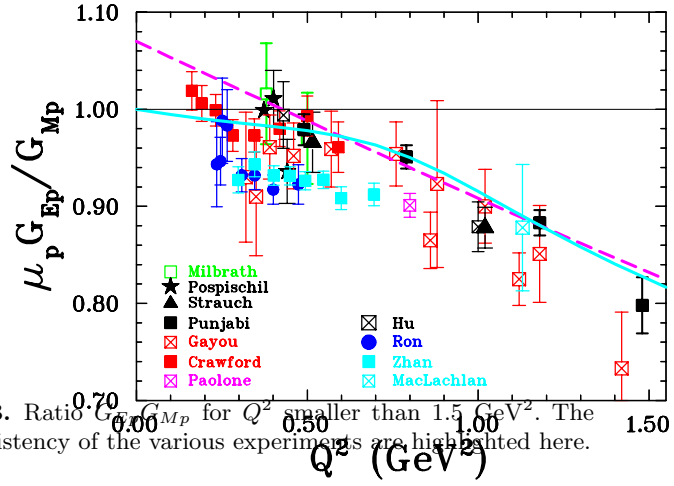

Fig. 3. Ratio G_{Ep}/G_{Mp} for Q^2 smaller than 1.5 GeV^2. The inconsistency of the various experiments are highlighted here.

1.2.1 Proton Radius

In a general sense the elastic *ep* cross section is related to the Mott cross section for a spin $\frac{1}{2}$ electron without internal structure times the Fourier transform of the charge

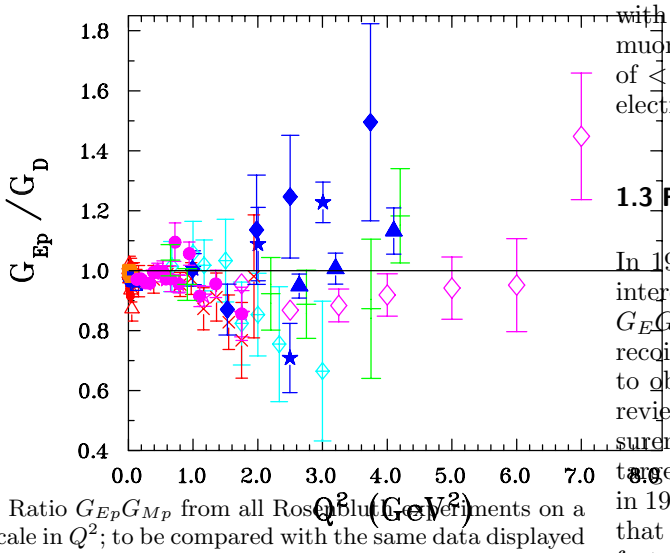

Fig. 4. Ratio $G_{Ep}G_{Mp}$ from all Rosenbluth experiments on a linear scale in Q^2; to be compared with the same data displayed on a log scale.

and/or magnetization density of the target nucleon as follows:

$$\sigma(\theta_e) = \sigma_{Mott} \times \left| \int_{volume} \rho(\boldsymbol{r}) exp i\boldsymbol{q}.\boldsymbol{r} d^3\boldsymbol{r} \right|^2 \qquad (12)$$

where $\rho(\boldsymbol{r})$ is either the electric- or the magnetic spacial distribution function. If follows, for the particular of the electric form factor $G_{Ep}(Q^2)$, that for short distances it can be expanded in terms of even moments of the distance $< r_e^{2n} >$ as:

$$G_{Ep} = 1 - \frac{1}{6}Q^2 < r_e{}^2 > + \frac{1}{120}Q^4 < r_e{}^4 > ... \qquad (13)$$

Hence for very small distance within the nucleon, the mean-square radius of the proton can be obtained from the derivative of Eq. 13

$$\frac{dG_{Ep}}{dQ^2} = -\frac{1}{6}|left r_e{}^2|right_{atQ^2=0} \qquad (14)$$

from which follows the relation

$$< r_e{}^2 >= -6|left \frac{dG_{Ep}}{dQ^2}|right_{atQ^2=0}; \qquad (15)$$

A similar relation holds for the magnetic radius $< r_m{}^2 >$. Many electron scattering experiments have obtained values of $< r_e{}^2 >$ by fitting low Q^2 cross section data [74,75] ; $< r_m{}^2 >$ is more difficult to obtain as its contribution to the cross section is weighted down by the factor τ (see Equ. 9).

The proton radius can also be obtained from precise measurements of the Lamb shift energies either in the hydrogen atom (Ref. [60]), or in muonic hydrogen (Ref. [7]). In both cases the 2S-2P Lamb shift is affected by the fact that the S-state wave function is maximum at the hydrogen's center, while the P-state has minimal overlap with the hydrogen nucleus. Recent measurements of the muonic Lamb shift energies at PSI have produced values of $< r_e{}^2 >$ which are smaller than the mean value of all electron scattering experiments by 7 σ ([66]).

1.3 Formalism of double polarization experiments

In 1968 and 1974 Akhiezer and Rekalo [4] discussed the interest of measuring an interference term of the form $G_E G_M$ by measuring the transverse component of the recoiling proton polarization in $\boldsymbol{ep} \rightarrow e\boldsymbol{p}$ at large Q^2, to obtain G_E in the presence of a dominating G_M. In a review paper Dombey [61] emphasized the virtues of measurements with a polarized lepton beam on a polarized target to obtain polarization observables. Also much later in 1982 Arnold, Carlson and Gross [68] discussed in detail, that the best way to measure the neutron and proton form factors would be to use the ${}^2H(\boldsymbol{e}, e'\boldsymbol{n})n$ and ${}^1H(\boldsymbol{e}, e'\boldsymbol{p})$ reactions, respectively.

Indeed, both the recoil polarization and target asymmetry measurement methods have been used successfully to measure the proton and neutron form factors to high four momentum transfer, Q^2, at Jefferson Lab. These methods have been used also at MIT-Bates, the Mainz Microtron (MAMI),and Nationaal Instituut voor Kernfysica en Hoge Energie Fysica (NIKHEF), to make precise proton and neutron form factor measurements at lower Q^2. Both methods are discussed below, with benefits and drawbacks of using polarized target and focal plane polarimeter.

1.3.1 Recoil polarization method

With a longitudinally polarized electron beam and an unpolarized hydrogen target, the polarization of the incoming electron is transferred to the proton via an exchange of a virtual photon as shown in Fig. 5. For elastic ep scattering with a longitudinally polarized electron beam, the only non-zero polarization transfer observables are the longitudinal and transverse polarizations, P_ℓ and P_t. For single photon exchange, the transferred polarization can be written in terms of the Sachs form factors as:

$$\begin{aligned} I_o P_n &= 0 \\ I_o P_\ell &= h P_e \frac{(E_{beam} + E_e)}{M} \sqrt{\tau(1+\tau)} \tan^2 \frac{\theta_e}{2} G_M^2 \\ I_o P_t &= -h P_e 2\sqrt{\tau(1+\tau)} \tan \frac{\theta_e}{2} G_E G_M \end{aligned} \qquad (16)$$

where $h = \pm 1$ and P_e are the beam helicity and polarization, respectively; E_{beam} and E_e are the incident and scattered electron energies, θ_e is the electron scattering angle, and M is the mass of the proton; $I_o = G_E^2 + \frac{\tau}{\epsilon} G_M^2$, is the unpolarized cross section and $\epsilon = [1 + 2(1+\tau)\tan^2 \frac{\theta_e}{2}]^{-1}$ is the longitudinal polarization of the virtual photon.

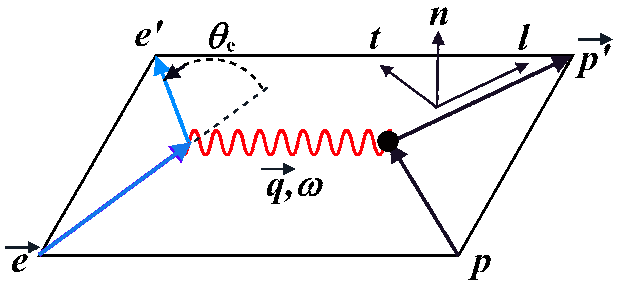

Fig. 5. Illustration of the kinematics and polarization of the recoil proton for $\boldsymbol{ep} \to e'\boldsymbol{p}$.

The ratio of G_E and G_M is then directly obtained from the ratio of the two polarizations P_t and P_ℓ components:

$$\frac{G_E}{G_M} = -\frac{P_t}{P_\ell}\frac{(E_{beam}+E_e)}{2M}\tan(\frac{\theta_e}{2}). \qquad (17)$$

In the one-photon exchange process, the form factors depend only on Q^2 and a deviation from constant would indicate a mechanism beyond the Born approximation. For each Q^2, a single measurement of the azimuthal angular distribution of the proton scattered in a secondary target gives both the longitudinal and transverse polarizations. Thus the ratio of electric to magnetic form factors of the proton is obtained directly from a simultaneous measurement of the two recoil polarization components. The knowledge of the beam polarization and of the analyzing power of the polarimeter is not needed to extract the ratio, G_E/G_M. The kinematic factors in Eq. (17) are typically known to a precision far greater than the statistical precision of the recoil polarization components.

1.3.2 Asymmetry with polarized targets

It was discussed by Dombey [61] in a review paper in 1969 that the nucleon form factors can be extracted from the scattering of longitudinally polarized electrons off a polarized nucleon target. In the one photon exchange approximation, the elastic electron nucleon scattering cross section can be written reaction en as a sum of two parts: Σ, which corresponds to the unpolarized elastic differential cross section $d\sigma/d\Omega_e$, and a polarized part Δ, which is non-zero only if the electron beam is longitudinal polarized [76,2];

$$\sigma_h = \Sigma + h\Delta, \qquad (18)$$

where h is the beam helicity, and Σ the unpolarized elastic ep cross section can be written as:

$$\Sigma = \left(\frac{d\sigma}{d\Omega}\right)_{Mott}\frac{E_e}{E_{beam}}\frac{1}{1+\tau}\left[G_E^2 + \frac{\tau}{\epsilon}G_M^2\right]. \qquad (19)$$

The polarized part of the cross section, Δ, with two terms related to the directions of the target polarization,

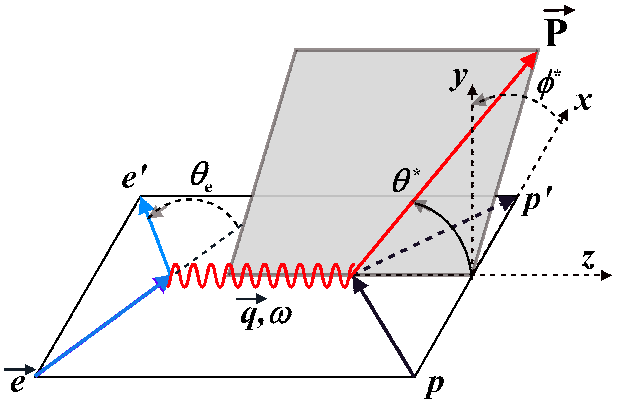

Fig. 6. Illustration of the kinematics and orientation of the target polarization $\boldsymbol{P}$, for the reaction $\boldsymbol{en} \to e'n$.

$\boldsymbol{P}(\theta^*\phi^*)$, is given by [76,2]:

$$\Delta = -2\left(\frac{d\sigma}{d\Omega}\right)_{Mott}\frac{E_e}{E_{beam}}\tan\frac{\theta_e}{2}\sqrt{\frac{\tau}{1+\tau}}\left(\sqrt{\tau\left[1+(1+\tau)\tan^2\frac{\theta_e}{2}\right]}\cos\theta^* G_M^2 + \sin\theta^*\cos\phi^* G_E G_M\right) \qquad (20)$$

where θ^* and ϕ^* are the polar and azimuthal laboratory angles of the target polarization vector with $\boldsymbol{q}$ in the $\boldsymbol{z}$ direction and $\boldsymbol{y}$ normal to the electron scattering plane, as shown in Figure 6.

The physical asymmetry A is then defined as

$$A = \frac{\sigma_+ - \sigma_-}{\sigma_+ + \sigma_-} = \frac{\Delta}{\Sigma}, \qquad (21)$$

where σ_+ and σ_- are the cross sections for the two beam helicities.

For a longitudinally polarized beam and polarized target, the measured asymmetry, A_{meas}, is related to the physical asymmetry, A, by

$$A_{meas} = P_{beam}P_{target}A, \qquad (22)$$

where P_{beam} and P_{target} are electron beam and target polarization, respectively, and A can be obtained using Eqs. (19) and (20),

$$A = -\frac{2\sqrt{\tau(1+\tau)}\tan\frac{\theta_e}{2}}{G_E^2 + \frac{\tau}{\epsilon}G_M^2}\left[\sin\theta^*\cos\phi^* G_E G_M + \sqrt{\tau\left[1+(1+\tau)\tan^2\frac{\theta_e}{2}\right]}\cos\theta^* G_M^2\right]. \qquad (23)$$

From Eq. (23), it is apparent that to extract G_E, the target polarization in the laboratory frame must be perpendicular with respect to the momentum transfer vector $\boldsymbol{q}$ and within the reaction plane, with $\theta^* = \pi/2$ and $\phi^* = 0^o$ or 180^o. For these conditions, the physical asymmetry A in Eq. (23) simplifies to:

$$A_{perp} = \frac{-2\sqrt{\tau(1+\tau)}\tan\frac{\theta_e}{2}\frac{G_E}{G_M}}{(\frac{G_E}{G_M})^2 + \frac{\tau}{\epsilon}}. \qquad (24)$$

As $(G_E/G_M)^2$ is quite small, A_{perp} is approximately proportional to G_E/G_M. In practice, the second term in Eq. (23) is not strictly zero due to the finite acceptance of the detectors, but these effects are small and depend on kinematics only in first order and can be corrected for, so the ratio G_E/G_M is not affected directly.

The discussion above is only applicable to a free electron-nucleon scattering. For a quasi-elastic electron scattering from a nuclear targets, like ^{2}H or ^{3}He, corrections are required for several nuclear effects.

1.4 Two-photon exchange

In the one-photon exchange process, the form factors depend only on Q^2 and a deviation from constant would indicate a mechanism beyond the Born approximation.

In the general case, elastic *ep* scattering can be described by three complex amplitudes [31,63]: $\tilde{G}_M$, $\tilde{G}_E$, and $\tilde{F}_3$, the first two chosen as generalizations of the Sachs electric and magnetic form factors, G_E and G_M, and the last one, $\tilde{F}_3$, vanishing in case of Born approximation. The reduced cross section, σ_{red}, and the proton polarization transfer components P_t and P_l, including two-photon exchange formalism, can be written as [63]:

$$\frac{\sigma_{red}}{G_M^2} = 1 + \frac{\varepsilon R^2}{\tau} + 2\frac{\Re\delta\tilde{G}_M}{G_M} + 2R\varepsilon\frac{\Re\delta\tilde{G}_E}{\tau G_M} + 2\left(1+\frac{R}{\tau}\right)\varepsilon Y_{2\gamma} \quad (25)$$

$$P_t = -\sqrt{\frac{2\varepsilon(1-\varepsilon)}{\tau}}\frac{G_M^2}{\sigma_{red}}\left(R + R\frac{\Re\delta\tilde{G}_M}{G_M} + \frac{\Re\delta\tilde{G}_E}{G_M} + Y_{2\gamma}\right) \quad (26)$$

$$P_l = \sqrt{(1-\varepsilon^2)}\frac{G_M^2}{\sigma_{red}}\left(1 + 2\frac{\Re\delta\tilde{G}_M}{G_M} + \frac{2}{1+\varepsilon}\varepsilon Y_{2\gamma}\right), \quad (27)$$

where:

$$\Re\tilde{G_M}(Q^2,\varepsilon) = G_M(Q^2) + \Re\delta\tilde{G_M}(Q^2,\varepsilon) \quad (28)$$

$$\Re\tilde{G_E}(Q^2,\varepsilon) = G_E(Q^2) + \Re\delta\tilde{G_E}(Q^2,\varepsilon) \quad (29)$$

$$R(Q^2) = G_E(Q^2)/G_M(Q^2)$$

Here $\tau = Q^2/4M_p^2$, and $\varepsilon = [1 + 2(1+\tau)\tan^2\frac{\theta_e}{2}]^{-1}$, where θ_e is the lab electron scattering angle. While the Sachs form factors depend only on Q^2, in the general case the amplitudes depend also on ε. The reduced cross section and the transferred proton polarization components are sensitive only to the real part of the amplitudes.

In Born approximation only the first term remains in the reduced cross section, σ_{red}, and the proton polarization transfer components P_t and P_l are :

$$\sigma_{red}/G_M^2 = 1 + \frac{\varepsilon R^2}{\tau} \quad (30)$$

$$P_t = -\sqrt{\frac{2\varepsilon(1-\varepsilon)}{\tau}}\frac{G_M^2 R}{\sigma_{red}}, \quad (31)$$

$$P_l = \sqrt{(1-\varepsilon^2)}\frac{G_M^2}{\sigma_{red}} \quad (32)$$

2 Recent developments; to be relocated

The experimental and theoretical situation for the nucleon form factors were reviewed extensively in the 7 years following publication of the results of the first recoil polarization experiment at Jefferson Lab [57]. Chronologically these reviews include Gao [39], Hyde-Wright et al. [19], Perdrisat et al. [65] and Arrington et al. [20], Arrington et al [8], Cloet et al. [25] and Perdrisat and Punjabi [64]. At this point in time, the double-polarization method had been used up to 5.6 GeV^2 for the proton form factor ratio G_{Ep}/G_{Mp} ([57,78,**?**], and 1.45 GeV^2 for G_{En}/G_{Mn}. Recent polarization experiments at JLab for G_{Mn} to a Q^2 of 0.6 GeV^2 [9] had been published, and a mix of polarization and cross section had been obtained up to 5 GeV^2 for G_{Mn}, the latest using the cross section ratio method, to obtain G_{Mn} from the measured $\frac{\frac{d\sigma}{d\Omega}[^2H(e,e'n)_{QE}]}{\frac{d\sigma}{d\Omega}[^2H(e,e'p)_{QE}]}$ ratio [79].

The principal revelation coming out of the first G_{Ep}/G_{Mp} experiment using recoil polarization was the systematic decrease of this ratio with increasing Q^2. There existed data from the 1970's which suggested a similar behavior, although they were limited to Q^2 smaller than 3 GeV^2, and had large uncertainties. Interestingly, at that time, models based on vector meson dominance (VMD) [**?**,36, 56] were predicting a rapid decrease of the ratio G_{Ep}/G_D, reaching a value of 0.5 at Q^2 of 4 GeV/c. In the same period, a first paper from the Stanford group [49] suggested a drastically different Q^2 dependence of the same ratio, G_{Ep}/G_{Mp}, with values reaching 1.35+/-0.3 at Q^2=3.6 GeV^2 (verify these numbers). The complete set of experimental results derived from cross section measurements is shown in Fig. 3 and 8. It includes the most recent JLab results of [55,45].

Since the last review paper was published, considerable theoretical work was performed. Some of the original models discussed in the 1970's, in particular the original Vector Dominance (VMD), as well as the Constituent Quark (CQM) models were revisited, made relativistic, then more of less left the front row, with the exception of Lomon [51], Bijker [67] and others.

The proton form factors were originally introduced in non-relativistic scattering, as the three-dimensional Fourier transform of the charge density [44,70]. However the proton recoil implies that the electron is interacting with a moving charge distribution. Already for Q^2=0.25 GeV^2, the recoil proton relativistic boost factor γ is 1.1, corresponding to $v/c = 0.41$. The argument that form factors are Fourier transforms of nucleon density in the Breit frame was abandoned, as this frame's velocity in the Lab frame is different for every Q^2.

The proton in its ground state is not necessarily spherically symmetric, but can show a typical multipole shape,

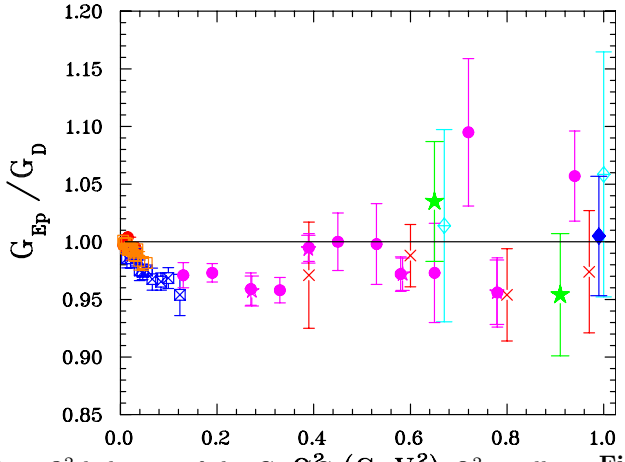

Fig. 7. Low Q^2 behavior of the G_{Rp}/G_D ratio for Q^2 smaller than 1 GeV^2 for Rosenbluth data, illustrating the very small deviation from a constant of this ratio for small Q^2.

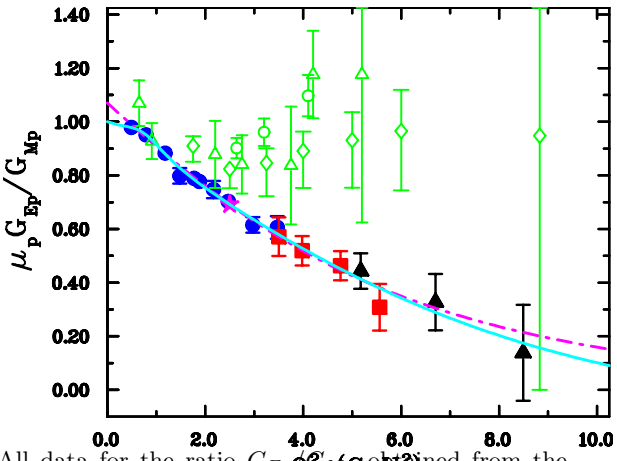

Fig. 9. All data for the ratio G_{Ep}/G_M obtained from the three large Q^2 recoil polarization experiments at JLab. The dot-dashed curve is a 4 parameter fit without constrain at Q^2=0, the solid line is a 7 parameter fit with ratio constrained to 1 at Q^2=0; Both fits are of the Kelly type, polynomial over polynomial, with $1/Q^2$ behavior at large Q^2.

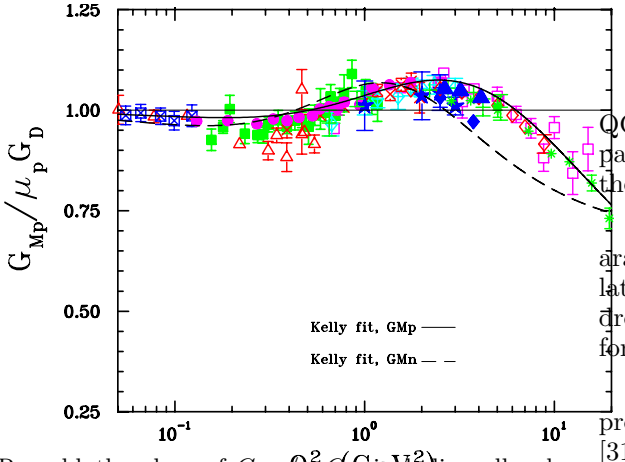

Fig. 8. Rosenbluth values of $G_{Mp}/\mu_p G_D$ including all published data, for comparison with Fig. 1.

when referred to the spin direction of one of its quarks (constituents) relative to the nucleon spin orientation [35].

The wave front or infinite momentum frame densities are invariant, two-dimensional transverse charge and magnetization distribution, and are drastically different from the non-relativistic ones [?,?].

Elastic ep scattering in the 1 to 10 GeV^2 range of 4-momentum squared transfer is the domain of non-perturbative quantum chromodynamics (QCD); as a consequence of Dynamical Chiral Symmetry Breaking, valence quarks acquire a mass of order $M_p/3$ in the infrared limit. [?,25]

Scaling as a consequence of Perturbative QCD may have visible consequences even in the non-perturbative domain [?]

The di-quark structure of the nucleon has observable consequences [?]

The mass of the dressed quarks originates from the QCD vacuum; it results from accretion of quark-antiquark pairs from decaying gluons spontaneously emerging from the vacuum [25].

Assuming isospin symmetry one can obtain flavor separated dressed quark form factors from simple linear relations between the Dirac and Pauli form factors. The dressed up and down quarks have significantly different form factors [25,?,?,?,?,?].

A zero crossing of GEp, if and when observed, would provide information on the dressed-quark mass function [31].

Nucleon form factors determine the parameters of the valence quark GPDs; these can be used to obtain corresponding valence quark densities [31].

The available data suggest that the isovector electric form factor (GEp-GEn) has a zero near Q^2 4.3 GeV^2; this feature can be predicted in lattice calculations, from the connected diagram only. [31].

Soft Collinear Effective Theory (SCET), Kivel and Vanderhaeghen(2013) for two-photon exchange [?].

3 GEn; to be relocated

This in preparation for the neutron section, in particular fig with $\mu_n G_{En}/G_{Mn}$. Nov. 3/14.

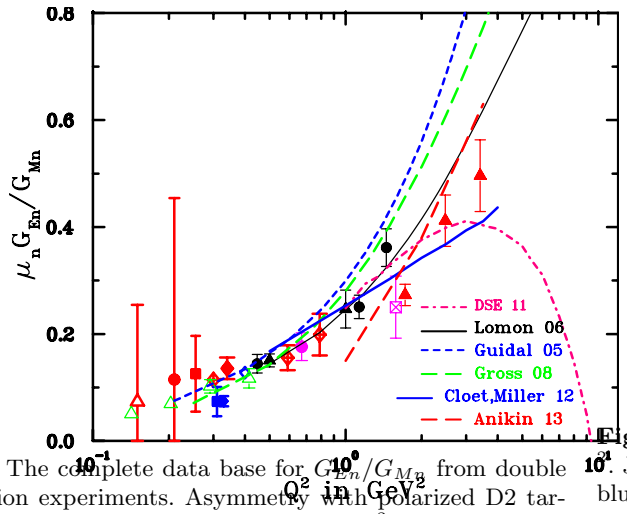

Fig. 10. The complete data base for G_{En}/G_{Mn} from double polarization experiments. Asymmetry with polarized D2 target: [46,40,37,?], asymmetry with polarized ^3He target: [21,1,?,47,29,48,?,71,?], recoil polarization with D2 target [33,22,59,?,69,11]

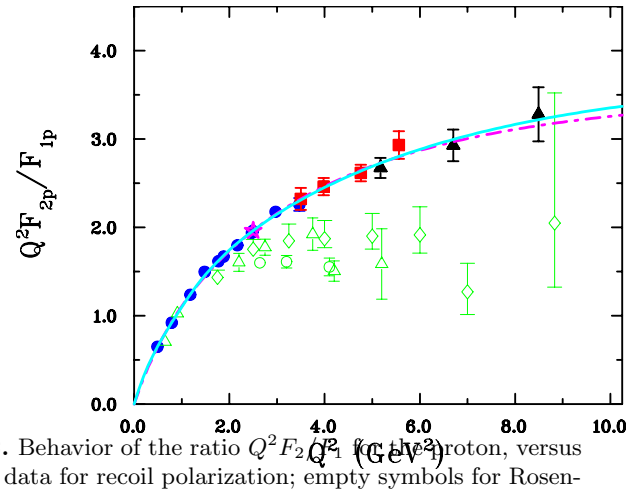

Fig. 12. Behavior of the ratio Q^2F_2/F_1 for the proton, versus Q^2. JLab data for recoil polarization; empty symbols for Rosenbluth data.

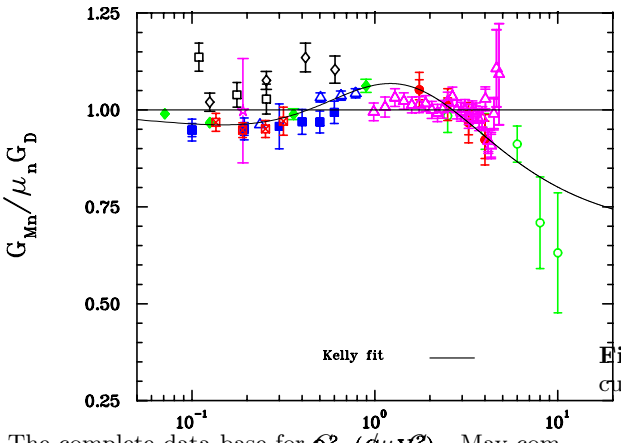

Fig. 11. The complete data base for $G_{Mn}/\mu_n G_D$. May compare with the equivalent figure for $G_{Mp}/\mu_p G_D$.

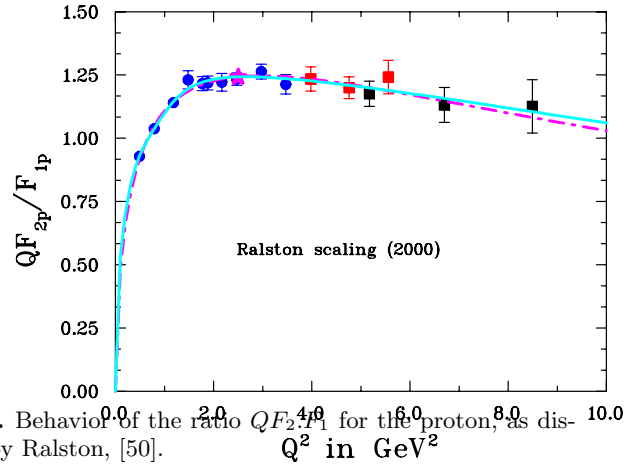

Fig. 13. Behavior of the ratio QF_2/F_1 for the proton, as discussed by Ralston, [50].

4 More Figures

5 Experimental Status

5.1 Electron Scattering Cross Section Experiments

A recent experiment at the Mainz Microtron measured precision elastic cross-sections over a range of $Q^2 = 0.003$ to 1.0 GeV^2.

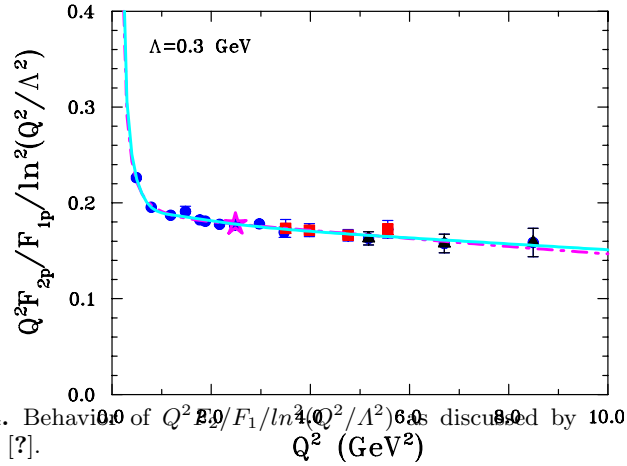

Fig. 14. Behavior of $Q^2F_2/F_1/ln^2(Q^2/\Lambda^2)$ as discussed by Belitsky [?].

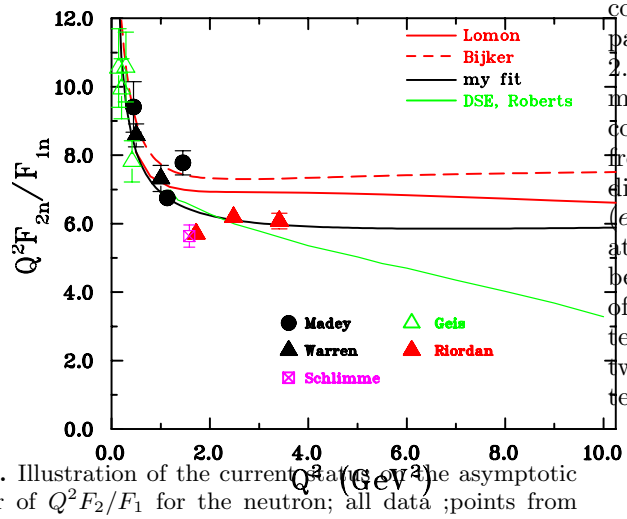

Fig. 15. Illustration of the current status of the asymptotic behavior of Q^2F_2/F_1 for the neutron; all data ;points from double polarization experiments. "My Fit" needs to be verified.

dependence on ϵ compared to (e, e') experiments. All this combines to reduce the ϵ dependent systematic error compared to (e, e'). The form factors were measured at $Q^2 =$ 2.64, 3.10 and 4.60 GeV^2. In the Figure, the measurements of $\mu G_p^E/G_p^M$ from the (e, p) reactions are plotted compared to a global analysis of previous measurements from (e, e') experiments and the agreement between the different methods is excellent. The plotted errors for the (e, p) data set are the combined statistical and systematic error and the error on the extraction of $\mu G_p^E/G_p^M$ has been improved by factors of two to three. The detection of scattered electrons or the scattered protons experiment techniques has different systematics, so the agreement between the two techniques indicate that experimental systematic error are understood.

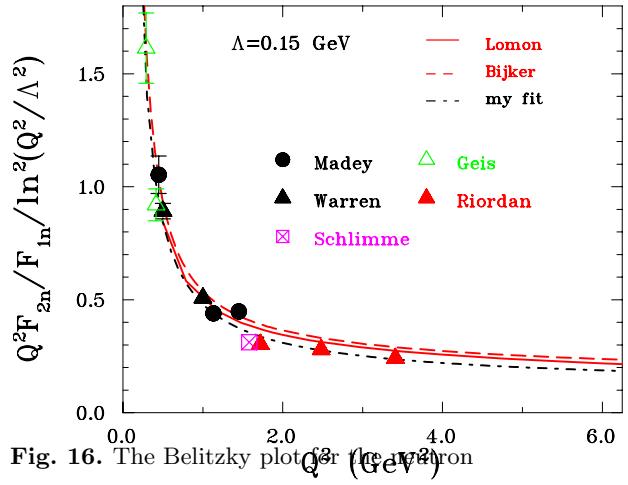

Fig. 16. The Belitzky plot for the neutron

5.1.1 G_p^M - Dipole Form Factor Parametrization

5.1.2 G_p^E - Elastic Scattering Results

5.1.3 SuperRosenbluth Separation Results

Taking advantage of the high duty factor of modern accelerators, cross-sections can be measured to high precision over a range of ϵ in a relative short time period. Instead of detecting the elastically scattered electron, (e, e'), an experiment which detected the elastically scattered proton to identify elastic reactions, (e, p), was run at Jefferson Lab in 2002. The same experimental approach of extraction the form factors by measuring elastic cross-sections at fixed Q^2 and different ϵ by varying the beam energy is used. The experimental method takes advantage of the fact that the proton momentum is constant for all epsilon at a fixed Q^2. In addition for (e, p) , the detected proton rate and the radiation corrections have a smaller

With the success of the first Jefferson Lab (e, p) experiment, a subsequent experiment was run at Jefferson Lab in Hall C. The experiment measured cross-sections at a total of 102 kinematic settings covering a wide Q^2 range from 0.4 to 5.76 GeV^2 with at least three ϵ points per Q^2. The emphasis was at each Q^2 to measure as wide an ϵ range as possible. At $Q^2 = 1$ GeV^2, thirteen ϵ points were measured ranging from ϵ =0.05 to 0.98, with eight of the points above $\epsilon = 0.8$. Similarly for At $Q^2 = 2.3$ GeV^2, ten ϵ points were measured ranging from ϵ =0.07 to 0.92, with five of the points above $\epsilon = 0.7$. The wide range of ϵ at a fixed Q^2 allows a check of the non-linearity in the ϵ dependence of the cross-section which would be a sign of two-photon exchange reactions effecting the cross-sections. The effects from two-photon exchange could have a dramatic ϵ dependence near $\epsilon = 1$.

6.1.1 Conformal fits to Form Factors

There has been a lively, at least to those engaged in it, discussion of what sorts of functions to use in fitting the form factors. Simple polynomial fits, for example, will not converge for moderate or large momentum transfers. The reason flows from the fact that the form factors are, from a mathematical viewpoint, analytic functions of their argument $Q^2 = -q^2$, except for cuts at known locations. The cuts are on the timelike side, and begin where one can have a photon to two pion transition at $q^2 = 4m_\pi^2$. A cut can be viewed as a weighted continuum of poles, so that there is a contribution to the form factor containing a factor $1/(q^2 - 4m_\pi^2)$. The weighting of this pole may be weak, but in principle its existence means that a polynomial expansion of the form factor will not converge for $Q^2 \geq 4m_\pi^2$. It is like the expansion of the geometric series $1/(1-x)$, which does not converge for $|x| \geq 1$; simply replace x by $q^2/(4m_\pi^2)$.

However, it is possible to make a mapping of Q^2 to another variable, denote it z, where a polynomial expansion in z is allowed. The trick is to find a transformation where spacelike momentum transfers all map onto the real line $|z| < 1$ and timelike momentum transfers map onto the circle $z = 1$ (in the complex z-plane). Then since all poles of the form factors lie on the unit circle in z, a polynomial expansion in z is convergent everywhere inside the unit circle, *i.e.,* for all spacelike momentum transfers.

This trick has been applied in the context of Weak interaction form factors, as for semileptonic meson decay, for some time [18,17]. It has more recently been applied to fitting electromagnetic form factors [42,53].

The variable z can be given by the conformal mapping [42,53], with $t = q^2$,

$$z(t, t_{\rm cut}) = \frac{\sqrt{t_{\rm cut} - t} - \sqrt{t_{\rm cut}}}{\sqrt{t_{\rm cut} - t} + \sqrt{t_{\rm cut}}}\,, \tag{33}$$

where $t_{\rm cut} = 4m_\pi^2$ and one can easily enough verify that the mapping has the properties stated above.

Fitting with a nonconvergent expansion can give good analytic fits to the data in any region where there is data to be fit. The danger lies in extending them outside the region where there is data. Such extrapolations can go awry, sometimes diverging wildly from physical expectation and sometimes, depending on how far one extrapolates, there may be problems that are less visible. Here enters also the proton radius question, whose evaluation from form factors requires an extrapolation from the lowest Q^2 where there is data down to $Q^2 = 0$. Extrapolating a fit made with an intrinsically convergent expansion is arguable safer.

The two fits made to the electromagnetic form factors using the conformal variable z, however, differ in their conclusions regarding the proton charge radius. The earlier fit [42] used electron-proton scattering data available before the Mainz experiment [14] published in 2010. They found a proton radius $R_E^p = 0.870 \pm 0.023 \pm 0.012$, so their central value is closer to the CODATA value than to the muonic Lamb shift value. The other fit [53] used the 1422 data points from the Mainz experiment, and obtained $R_E^p = 0.840 \pm 0.015$ fm (see also [54]).

6.1.2 Vector Meson Dominance and Dispersion Analyses

Newer works here include the dispersive analyses of the nucleon form factors by workers in Bonn [52–54]. These works include general analyses and fits to the form factors, as well as aspects directly aimed at the resolution of the proton radius puzzle [52–54].

6.1.3 Constituent Quark Models

6.1.4 Pion Cloud Models

6.2 Dyson-Schwinger Equations and Diquark Models

The Dyson Schwinger equations (DSE) are generically a non-perturbative approximation for obtaining results for a field theory, in the present case QCD. The equations

are, in principle, an infinite set of coupled integral equations. In practice, they must be truncated, in a way that preserves all symmetries of QCD, in order to proceed with any calculation. For a general DSE review, see [12]. Important results early in the program include a representation for the dressed quark propagator that includes a quark mass function, $M(p^2)$, depending on the momentum p of the propagator. Also early on in the program is building a model of the quark-quark and quark-antiquark interactions that will reproduce data on, among other quantities, the pion electromagnetic form factors and the pion distribution amplitude.

One then develops a three quark wave function model for the nucleon by solving the three-cody Fadeev equations and using the based on the same interaction as was used for the pion. There arise significant diquark, *i.e.,* significant quark-quark correlations, that have a strong effect on the form factors one obtains. The quarks in this model are dressed, so that many of their features are quite different from expectations for pointlike fermions. One finds in particular large quark anomalous chromomagnetic moments, which affect the quark-gluon interactions, which lead to large quark anomalous magnetics moments in the quark-photon interactions, which in turn are needed to obtain good fits to the nucleon electromagnetic form factor data.

The theoretical DSE results [26,24,23] show the falloff of the G_E^p/G_M^p ratio that is seen in the data. The authors also note that there is sensitivity of the form factor results to the parameters of the model, affected also for example the detailed $M(p^2)$ function for p in the few GeV range, which can be turned into a feedback procedure for tuning the bound state model.

The sources so far consulted do not contain the high Q^2 normalization of the form factors, or detailed direct information about how the quark angular momentum is affecting the form factor results.

However, we may mention that models based on the Dyson-Schwinger equations do extend to form factors for other hadronic reactions, such as the electromagnetic $N \rightarrow \Delta$ transition [72,73]. The result for the ratio of the electric and magnetic transition form factors for this process, R_{EM}, turns out to be small in the DSE approach, even out to momentum transfers above 5 GeV^2, in accord with experimental data. The perturbative QCD result, that $R_{EM} \rightarrow 1$ does come out, but only at momentum transfers that are extremely high. The mechanism that keeps R_{EM} small is not stated in the presentations currently available.

6.3 Links between Deep-Inelastic Scattering and Nucleon Form Factors

6.4 Lattice QCD Calculations of Nucleon Form Factors

Strictly speaking, lattice calculations of nucleon form factors are currently available only for the isovector form factors.

Isoscalar form factors require calculations of disconnected diagrams, which are diagrams with quark loops not connected to the quark lines emanating from or ending on the lattice nucleon source or sink. There are gluons that attach the quark loops to the valence quarks, but these are not indicated in lattice diagrams, hence the phrase "disconnected." Contributions from the disconnected loops require computer time intensive calculations, and the calculations remain undone. However, the disconnected diagrams contribute equally to proton and neutron, so the isovector case can be considered without them.

A review including lattice form factor results up to 2010 is available in [41], and new lattice form factor results are reported in [6,15,38].

The new calculations have pion masses from 373 MeV down to a close to physical 149 MeV in [38]. The latter also strove to reduce contamination from excited nucleons. They analyze their lattice data using three methods which they call the standard ratio method, the summation method, and the generalized pencil-of-function method (GPoF), with varying outcomes. The best results, judged by comparison to data as represented by one of the standard fits [5], come from the summation method. Here agreement with experimental data is good for both G_E^v and G_M^v in the region considered, which is Q^2 from scattering threshold up to about 0.5 GeV^2, with uncertainty limits about 20% at Q^2 of 0.4 GeV^2,

Refs. [6,15] have pion masses in the 213–373 MeV range, and quote results for somewhat higher Q^2. For Q^2 above about 0.6 GeV^2, their isovector form factors results tend to be 50% or so above the data for G_E^v (or F_1^v), with uncertainties indicated at about 10%. For G_M^v (or F_2^v) the results are closer to data . The authors of these works do point out that the lattice treatments with these pion masses are all consistent with each other.

One may specifically focus on nucleon radii calculated from lattice gauge theory. In the future, it may be possible and desirable to calculate using a dedicated correlator which gives directly the slope of the form factor at zero momentum transfer. Finding such correlators by taking derivatives of known correlators is suggested and studied [30] for lattice calculations of form factors at points where the Lorentz factors they multiply go to zero. Applications in [30] are to form factors for semi-leptonic scalar meson decay, and to hadronic vacuum polarization corrections to the muon $(g-2)$.

At present, lattice calculations of nucleon radii proceed by calculating the form factor at several non-zero Q^2, fitting to a suitable form, typically a dipole form, and finding the radius by extrapolating to zero Q^2. Truly complete results are available only for the isovector nucleon. Ref. [38] presents a plot of radius results for lattice calculations at various pion masses. They use the Dirac radius, obtained from the slope of F_1^v, rather than the charge radius, but these are related by, using the proton as an example,

$$\langle r_{1p}^2 \rangle = \langle r_{Ep}^2 \rangle - \frac{3}{2}\frac{\kappa_p}{m_p^2}\,. \tag{34}$$

Hence, given the great accuracy of the magnetic moment measurements, one knows the Dirac radii to the same accuracy as the charge radii.

The great interest is obtain sufficient accuracy from the lattice results to be able to adjudicate between the electron and muon measured values of the isovector charge or Dirac radii. The electron measured isovector radius is straightforward to look up, the muon measured value of the Dirac or charge radius is for now a defined quantity obtained by using the electron value for the neutron radius-squared. Using the summation method, Ref. [38] obtain, by extrapolation to the physical pion mass, a value of the isovector Dirac radius between the muonic and electronic results, with uncertainties that accommodate both at about the one standard deviation level. However, using the GPoF or ratio method gives a smaller $\langle r_1^2 \rangle^v$, on the order of 2/3 the value from the summation method.

One may say there opportunity for further work. An uncertainty of 1% or less for the proton alone is needed for a lattice calculation to impact the proton radius puzzle.

References

1. A. K. Thompson, *et al.* and " Phys. Rev. Lett.$\tilde{6}$8 the neutron's form factors. 2901. 1992.
2. Ann. Phys. 191 A. S. Raskin, T. W. Donnelly. 78. 1986.
3. A. I. Akhiezer and " Sov. J. Part. Nucl.$\tilde{4}$ M. P. Rekalo, effects in the scattering of leptons by hadrons. 277. 1974. ; Fiz. Elem. Chast. Atom. Yadra 4 (1973) 662. FECAA,4,662;
4. A. I. Akhiezer and " Sov. Phys. Dokl.$\tilde{1}$3 M. P. Rekalo, phenomena in electron scattering by protons in the high energy 572. 1968. ; Dokl. Akad. Nauk Ser. Fiz. 180 () 1081. DANKA,180,1081;
5. W.M. Alberico, S.M. Bilenky, C. Giunti, and K.M. Graczyk. Electromagnetic form factors of the nucleon: New Fit and analysis of uncertainties. *Phys.Rev.*, C79:065204, 2009.
6. C. Alexandrou, M. Constantinou, S. Dinter, V. Drach, K. Jansen, et al. Nucleon form factors and moments of generalized parton distributions using $N_f = 2 + 1 + 1$ twisted mass fermions. *Phys. Rev.*, D88(1):014509, 2013.
7. Aldo Antognini, Franz Kottmann, Francois Biraben, Paul Indelicato, Francois Nez, et al. Theory of the 2S-2P Lamb shift and 2S hyperfine splitting in muonic hydrogen. *Annals Phys.*, 331:127–145, 2013.
8. John Arrington, Kees de Jager, and Charles F. Perdrisat. Nucleon Form Factors: A Jefferson Lab Perspective. *J.Phys.Conf.Ser.*, 299:012002, 2011.
9. Jefferson Lab E95-001 Collaboration factor from quasi-elastic 0.6-(GeV/c)**2 " Phys. Rev. C 75 B. Anderson, *et al.* 034003. 2007.
10. Bates FPP collaboration electron scattering from the " Phys. Rev. Lett.$\tilde{8}$0 deuteron. 452. 1998. ; Phys. Rev. Lett. 82 (1999) 2221 (erratum).
11. electric to magnetic form factor ratio H-2(e(pol.)-e' n(pol.))H-1 reaction to Q**2 = Rev. C **73** B. Plaster, *et al.* 025205. 2006.
12. Adnan Bashir, Lei Chang, Ian C. Cloet, Bruno El-Bennich, Yu-Xin Liu, et al. Collective perspective on advances in Dyson-Schwinger Equation QCD. *Commun.Theor.Phys.*, 58:79–134, 2012.
13. E.J. Beise, M.L. Pitt, and D.T. Spayde. The SAMPLE experiment and weak nucleon structure. *Prog.Part.Nucl.Phys.*, 54:289–350, 2005.
14. J.C. Bernauer et al. High-precision determination of the electric and magnetic form factors of the proton. *Phys.Rev.Lett.*, 105:242001, 2010.
15. Tanmoy Bhattacharya, Saul D. Cohen, Rajan Gupta, Anosh Joseph, Huey-Wen Lin, et al. Nucleon Charges and Electromagnetic Form Factors from 2+1+1-Flavor Lattice QCD. *Phys. Rev.*, D89:094502, 2014.
16. J.C. Bizot. *Phys.Rev.*, B140:1387, 1965.
17. Claude Bourrely, Irinel Caprini, and Laurent Lellouch. Model-independent description of $B \to \pi \ell \nu$ decays and a determination of $|V(ub)|$. *Phys.Rev.*, D79:013008, 2009.
18. C. Glenn Boyd, Benjamin Grinstein, and Richard F. Lebed. Model independent determinations of $\bar{B} \to Dl\bar{\nu}, D^* l\bar{\nu}$ form-factors. *Nucl.Phys.*, B461:493–511, 1996.
19. and " Ann. Rev. Nucl. Part. Sci.$\tilde{5}$4 Compton Scattering. 217. 2004.
20. and " Ann. Rev. Nucl. Part. Sci.$\tilde{5}$4 Compton Scattering. J. 2004. Arrington, C.D. Roberts, J.M. Zanotti, arXiv:nucl-th/0611050 2006.
21. C. E. Jones-Woodward, *et al.* 571. 1991.
22. C. Herberg, *et al.* 131. 1999.
23. Ian C. Cloet and Craig D. Roberts. Explanation and Prediction of Observables using Continuum Strong QCD. *Prog.Part.Nucl.Phys.*, 77:1–69, 2014.
24. Ian C. Cloet, Craig D. Roberts, and Anthony W. Thomas. Revealing dressed-quarks via the proton's charge distribution. *Phys.Rev.Lett.*, 111:101803, 2013.
25. I.C. Cloet, G. Eichmann, B. El-Bennich, T. Klahn, and C.D. Roberts. Survey of nucleon electromagnetic form factors. *Few Body Syst.*, 46:1–36, 2009.
26. Ian C. Clot, Wolfgang Bentz, and Anthony W. Thomas. Role of diquark correlations and the pion cloud in nucleon elastic form factors. *Phys.Rev.*, C90:045202, 2014.
27. Phys. Lett. 470 D. Barkhuff, *et al.* 39. 1999.
28. D. G. Ravenhall Rev. Mod. Phys. 29 D. R. Yennie, M. M. Lévy. 144. 1957.
29. 4257. 1999.
30. G.M. de Divitiis, R. Petronzio, and N. Tantalo. On the extraction of zero momentum form factors on the lattice. *Phys. Lett.*, B718:589–596, 2012.
31. Markus Diehl and Peter Kroll. Nucleon form factors, generalized parton distributions and quark angular momentum. *Eur.Phys.J.*, C73:2397, 2013.
32. P.A.M. Dolph, J. Singh, T. Averett, A. Kelleher, K.E. Mooney, et al. Gas dynamics in high-luminosity polarized He-3 targets using diffusion and convection. *Phys.Rev.*, C84:065201, 2011.
33. T. Eden, R. Madey, W.M. Zhang, B.D. Anderson, H. Arenhovel, et al. Electric form-factor of the neutron from the H-2 (e (polarized), e-prime n (polarized)) H-1 reaction at Q**2 = 0.255-(GeV/c)**2. *Phys.Rev.*, C50:1749–1753, 1994.
34. D. Eyl, A. Frey, H.G. Andresen, J.R.M. Annand, K. Aulenbacher, et al. First measurement of the polarization transfer on the proton in the reactions H (e (polarized), e-prime p (polarized)) and D (e (polarized), e-prime p (polarized)). *Z.Phys.*, A352:211–214, 1995.
35. " Phys. Rev. C 68 G. A. Miller, 022201(r). 2003.
36. Nucl. Phys. B 114 G. Höhler, *et al.* 505. 1976.
37. Jefferson Lab E93-026 Collaboration of the neutron at Q**2 = 0.5-GeV/c**2 Lett.$\tilde{9}$2 G. Warren, *et al.* 042301. 2004.

38. J.R. Green, J.W. Negele, A.V. Pochinsky, S.N. Syritsyn, M. Engelhardt, et al. Nucleon electromagnetic form factors from lattice QCD using a nearly physical pion mass. 2014.
39. " Int. J. Mod. Phys. E 12 H. Y.Gao, form factors. 1. 2003. ; H.Y.Gao, Int. J. Mod. Phys. E 12 () 567 (erratum).
40. H. Zhu, *et al.* 081801. 2001.
41. Ph. Hagler. Hadron structure from lattice quantum chromodynamics. *Phys. Rept.*, 490:49–175, 2010.
42. Richard J. Hill and Gil Paz. Model independent extraction of the proton charge radius from electron scattering. *Phys.Rev.*, D82:113005, 2010.
43. R. Hofstadter. *Rev. Mod. Phys.*, 28:214, 1956.
44. R. Hofstadter, H.R. Fechter, and J.A. McIntyre. *Phys. Rev.*, 92:978, 1953.
45. Phys. Rev. Lett.˜94 I. A. Qattan, *et al.* 142301. 2005.
46. 4988. 1999.
47. E' N) At Medium Momentum Transfer " Eur. Phys. J. A 6 J. Becker, *et al.* 329. 1999.
48. Lett. B 564 target analyzing powers from n) scattering. 199. 2003.
49. Phys. Lett. B 31 J. Litt, *et al.* 40. 1970.
50. Phys.Rev. D 69 J. P. Ralston, P. Jain. 053008. 2004.
51. Phys. Rev. C 64 Lomon E. L. 035204. 2001.
52. I.T. Lorenz, H.-W. Hammer, and Ulf-G. Meissner. The size of the proton - closing in on the radius puzzle. *Eur.Phys.J.*, A48:151, 2012.
53. I.T. Lorenz and Ulf-G. Meißner. Reduction of the proton radius discrepancy by 3? *Phys.Lett.*, B737:57–59, 2014.
54. I.T. Lorenz, Ulf-G. Meißner, H. W. Hammer, and Y. B. Dong. Theoretical Constraints and Systematic Effects in the Determination of the Proton Form Factors. 2014.
55. Phys. Rev. C 70 M. E. Christy, *et al.* 015206. 2004.
56. Z. Phys. A 322 M. F. Gari, W. Krümpelmann. 689. 1985. ; Phys. Lett. B 274 (1992) 150; Phys. Lett. B 282 (1992) 483(E).
57. M. K. Jones *et al.*, Jefferson Lab Hall A Collaboration. *Phys. Rev. Lett.*, 84:1398, 2000.
58. M. N. Rosenbluth. *Phys. Rev.*, 79:615, 1950.
59. M. Ostrick, *et al.* 276. 1999.
60. Kirill Melnikov and Timo van Ritbergen. The Three loop slope of the Dirac form-factor and the S Lamb shift in hydrogen. *Phys.Rev.Lett.*, 84:1673–1676, 2000.
61. Rev. Mod. Phys. 41 N. Dombey. 236. 1969.
62. O. Gayou *et al.*, Jefferson Lab Hall A Collaboration. *Phys. Rev. Lett.*, 88:092301, 2002.
63. " Phys. Rev. Lett.˜91 the polarization transfer method in measurement of the proton form factors. 142303. 2003.
64. C.F. Perdrisat and V. Punjabi. Nucleon Form Factors. 5(8)::10204, 2010.
65. C.F. Perdrisat, V. Punjabi, and M. Vanderhaeghen. Nucleon Electromagnetic Form Factors. *Prog.Part.Nucl.Phys.*, 59:694–764, 2007.
66. Randolf Pohl, Ronald Gilman, Gerald A. Miller, and Krzysztof Pachucki. Muonic hydrogen and the proton radius puzzle. *Ann.Rev.Nucl.Part.Sci.*, 63:175–204, 2013.
67. Phys Rev. C 69 R. Bijker, F. Iachello. 068201. 2004.
68. F. Gross Phys. Rev. C 23 R. G. Arnold, C. E. Carlson. 363. 1981.
69. E93-038 Collaboration e' n(pol.)) H-1 reaction Lett.˜**91** R. Madey, *et al.* 122002. 2003.
70. J. S. Levinger. 135. 1964.
71. S. Riordan, S. Abrahamyan, B. Craver, A. Kelleher, A. Kolarkar, et al. Measurements of the Electric Form Factor of the Neutron up to $Q^2 = 3.4GeV^2$ using the Reaction $^3He^{->}(e^{->}, e'n)pp$. *Phys.Rev.Lett.*, 105:262302, 2010.
72. Jorge Segovia, Chen Chen, Ian C. Clot, Craig D. Roberts, Sebastian M. Schmidt, et al. Elastic and Transition Form Factors of the $\Delta(1232)$. *Few Body Syst.*, 55:1–33, 2014.
73. Segovia, Jorge and Cloët, Ian C. and Roberts, Craig D. and Schmidt, Sebastian M. Nucleon and Δ Elastic and Transition Form Factors. *Few-Body Systems*, 55(12):1185–1222, 2014.
74. Ingo Sick. On the RMS radius of the proton. *Phys.Lett.*, B576:62–67, 2003.
75. Ingo Sick and Dirk Trautmann. Proton root-mean-square radii and electron scattering. *Phys.Rev.*, C89(1):012201, 2014.
76. Ann. Phys. 169 T. W. Donnelly, A. S. Raskin. 247. 1986.
77. Eur. Phys. J. A 12 Th. Pospischil, *et al.* 125. 2001.
78. 055202. 2005. ; Phys. Rev. C 71 () 069902 (erratum).
79. CLAS Collaboration to higher Q**2 " Nucl. Phys. A 755 W. K. Brooks, J. D. Lachniet. 261. 2005. ; Lachniet, unpublished, .